OCTOBER 01 2005

Acoustic analysis of a computer cooling fan

Lixi Huang; Jian Wang

J. Acoust. Soc. Am. 118, 2190–2200 (2005)
https://doi.org/10.1121/1.2010367

Acoustic analysis of a computer cooling fan

Lixi Huang[a] and Jian Wang
Department of Mechanical Engineering, The Hong Kong Polytechnic University, Kowloon, Hong Kong

(Received 29 September 2004; revised 3 July 2005; accepted 5 July 2005)

Noise radiated by a typical computer cooling fan is investigated experimentally and analyzed within the framework of rotor-stator interaction noise using point source formulation. The fan is 9 cm in rotor casing diameter and its design speed is 3000 rpm. The main noise sources are found and quantified; they are (a) the inlet flow distortion caused by the sharp edges of the incomplete bellmouth due to the square outer framework, (b) the interaction of rotor blades with the downstream struts which hold the motor, and (c) the extra size of one strut carrying electrical wiring. Methods are devised to extract the rotor-strut interaction noise, (b) and (c), radiated by the component forces of drag and thrust at the leading and higher order spinning pressure modes, as well as the leading edge noise generated by (a). By re-installing the original fan rotor in various casings, the noises radiated by the three features of the original fan are separated, and details of the directivity are interpreted. It is found that the inlet flow distortion and the unequal set of four struts make about the same amount of noise. Their corrections show a potential of around 10-dB sound power reduction. © *2005 Acoustical Society of America.* [DOI: 10.1121/1.2010367]

PACS number(s): 43.28.Ra, 43.50.Yw, 43.50.Gf [SFW] Pages: 2190–2200

I. INTRODUCTION

The problem of computer cooling fan noise is receiving increasing attention due to the continuous development of CPU power, and the trend of slim packaging. It may be said that, despite many unanswered questions, there is an abundance of general aeroacoustic knowledge regarding fan noise. However, to the best of the authors' knowledge, a detailed, systematic study on each component of the noise mechanism present in a specific type of cooling fan is yet to be reported. Using a typical computer cooling fan sample, the present experimental study aims to identify and quantify the exact source mechanisms in the fan assembly, and the directivity of the radiated sound. The emphasis is on the tonal noise but some preliminary results for the broadband noise are also reported. It is hoped that both qualitative and quantitative knowledge derived from such an experimental study would pave the way for further theoretical, computational modeling and, ultimately, design of a quiet computer cooling fan. In the remainder of this section, the relevant literature is briefly reviewed, followed by the description of the features of the sample fan.

In terms of general aeroacoustics research for rotating machines, Gutin (1936) was among the first to quantify the propeller noise caused by the rotation of steady loading, later called Gutin noise. Lighthill's (1952) acoustic analogy provided a formal platform of investigating aerodynamic sound, which was soon extended by Curle (1955) to include the effect of solid boundaries by replacing it with distributed dipoles while the explicit effect of acoustic scattering was neglected. It was not until Ffowcs Williams and Hawkings (1969) formally extended Lighthill's acoustic analogy by using the generalized functions to account for the effect of all solid boundaries in arbitrary motion. A comprehensive theoretical treatment of flow-induced noise was given by Blake (1986) and also by Howe (1998) in his recent monograph. The use of the so-called Ffowcs Williams and Hawkings' equation became a dominant feature from late 1970s in the field of acoustics for rotary machines. Generally speaking, there are three types of sources in a turbomachine or any machine with moving blades, monopole from the blade motion, dipole from fluctuating forces on blades, and quadrupole emanating from the core of turbulent jets. The sound power scales as the fourth, sixth, and eighth power of the representative flow speed for the three types of elementary sources, respectively. The tightly coupled monopoles on a rigid moving blade is effectively dipoles, and they are called thickness noise. For low speed applications, both thickness noise and the dipole related to the steady-flow loading, or Gutin noise, are unimportant when compared with the dipole arising from the unsteady flow features. Bulk turbulence noise is negligible, but its interaction with solid surface is not. As pointed out by Ffowcs Williams and Hall (1970), the scattering of convected boundary layer waves by a terminating edge of a half plane could generate powerful sound which scales as the fifth power of flow speed, and is known as the trailing edge noise. However, this reduction of the power exponent comes about as the solid surface provides a baffling effect. Such effect is absent and the power dependency goes back to the sixth when the blade is compact compared with the wavelength (Blake 1986). This is the case for the computer cooling fan being investigated here.

Focusing on the specific mechanisms at work in turbomachines and axial flow fans at subsonic speeds, it is found that the dominant noise source is often the unsteady pressure fluctuation arising from the interaction between rotating blades and stationary blades, or between rotating blades and steady but nonuniform incoming flow. Fitzgerald and Lauchle (1984) gave a comprehensive list of possible physi-

[a]Author to whom correspondence should be addressed; electronic mail: lixi.huang@polyu.edu.hk

cal mechanisms of noise radiation present in a subsonic fan. They have also made efforts to eradicate each one of these mechanisms and achieved success in noise reduction. Typical noise spectrum consists of a broadband superimposed by pure tones, mostly at the fundamental and the harmonics of the blade passing frequency (BPF). The dominant source for the pure tones is the interaction events. One of the most significant contributions was made by Tyler and Sofrin (1962), who revealed the important role played by the numbers of rotor and stator blades. The phenomenon of modal cut-off was discovered and shown to be consistent with duct acoustics. A contrast was made by Lowson (1970) between this cut-off behavior for the ducted fan and the acoustics of the unducted fan. He demonstrated that the radiation of the mismatched spinning modes cannot be cut off altogether but is rather reduced in acoustic efficiency. Kaji and Okazaki (1970), using the wake models of Kemp and Sears (1953, 1955), modeled the rotor-stator interaction with careful doublet arrays while preserving the blade effects on sound propagation in the duct and imposing Kutta conditions on trailing edges. Numerous studies on interaction noise were also conducted in the helicopter community. In most such studies, the focus has always been on the interaction between rotor and stator, and most noise is generated from the downstream part, namely the downstream stator or the rotor behind an inlet guidevane. The effect of a downstream stator on the upstream rotor is normally negligible in comparison. However, such effect seems to be the dominant noise source in the present study where the downstream stator are circular cylinders used to support a motor. The reason why the radiation from the downstream cylinders, or struts, is small compared with that from the upstream rotor blades is that the blades are so profiled to generate lifting forces while cylinders are not. The nature of the rotor-strut coupling in this case is mainly potential flow interaction, and the specific problem treated here represents a gap in literature.

In terms of the broadband noise, Sharland (1964) was one of the first to quantify it for axial-flow compressors. Three possible sources of broadband noise were described: the unsteady blade surface pressure arising from the turbulent boundary layer, lift fluctuation from the unsteady vorticity shed from the trailing edge, and random inlet flow fluctuations. The relationship between the first two mechanisms and the trailing edge noise described later by Ffowcs Williams and Hall (1970) was not clear at that point. Mugridge and Morfey (1972) also attempted to give an order of magnitude estimate for the broadband noise. A comprehensive review of earlier research was given by Morfey (1973). Longhouse (1976) categorized the tonal noise as rotational noise, and the broadband noise as nonrotational noise. His work demonstrated that design features good for reducing broadband noise could contradict those for discrete tones. Dominant nonrotational noise mechanisms are the vortex shedding from the blades and the tip clearance vortex interacting with the blade inner span or a neighboring blade. The former was studied in detail in Longhouse (1977) by using a rotor with very small tip clearance. It was shown that the vortex shedding can be suppressed by a leading edge serration which served as a vortex generator, and the resulting turbulent flow was less coherent and less efficient in radiating sound than the trailing edge scattering of instability waves in the laminar boundary layers in transition (Tollmien Schlichting, or TS, waves). It was proposed that Tollmien Schlichting waves are convected and magnified as they approach the trailing edge. The scattered sound initiates a disturbance back to the upstream TS waves forming a feedback loop. The noise radiated peaks at frequencies for which the distance between the transitional point and the trailing edge is an integer number of the TS wavelengths. The frequency of such discrete tone, as well as relative silence at other frequencies, has no bearing on the rotational speed of the fan, but a rigorous theory is yet to be formulated for such tones. Tip clearance noise is also regarded as the main mechanism of broadband noise by many researchers. Longhouse (1978) and Fukano *et al.* (1986) reported significant reductions of broadband noise when the clearance was minimized or a shroud was used. More recently, similar achievement was made by Quinlan and Bent (1998) albeit with some increase in low-frequency tonal noise. Apart from the two mechanisms described above, inlet flow turbulence is also regarded as a major contributor to the broadband noise although it serves as a tonal source at the same time when the turbulence scale is larger than the blade spacing. In most machines, the inlet flow passes through a contraction due to the bellmouth, and eddies present in the turbulent incoming flow get elongated as they squeeze through the tip clearance region of blades (Majumdar and Peake, 1998). Trunzo *et al.* (1981) investigated the sound radiated by the repeated chopping of such elongated eddies by the rotating blades. The tonal noise radiated was shown to be suppressed significantly when the eddies were broken up by an inlet grid at the expense of increased broadband noise. Majumdar and Peake (1998) treated the problem analytically in the context of quantifying the effect of ingested atmospheric turbulence during a ground based test of aeroengines.

Given such a variety of possible noise mechanisms, it would be of great practical interest to identify the dominant factor for a specific application. The current study focuses on the methodology of identifying such dominant noise source. For a computer cooling fan, much of the noise could be radiated by the interaction of the swirling exit flow and the cramped environment a cooling fan finds itself in. Nevertheless, the search for a quiet cooling fan has to start with a smooth flow condition when the fan operates in free space. A photograph of a typical cooling fan is shown in Fig. 1. As shown in the front view of Fig. 1(a), the fan has a rotor of seven well-profiled blades. The inner diameter of the casing is 9 cm, and the rotational speed is 3000 rpm when it is connected to a dc power supply of 12 V at a current of 0.4 A and operated at the free delivery condition. The inlet flow velocity is measured to be 5.1 m/s. The inlet has a bellmouth design with a straight slope of 5 mm in length, but the bellmouth is made incomplete by the square casing frame. The rotor is driven by a downstream motor attached to the casing via four struts, which are shown in the back view in Fig. 1(b). The lower left strut is larger than the rest in order to carry electric wiring. Figure 1(c) shows the top view (plane $x-y$) of the measurement plane with four symmetrical mi-

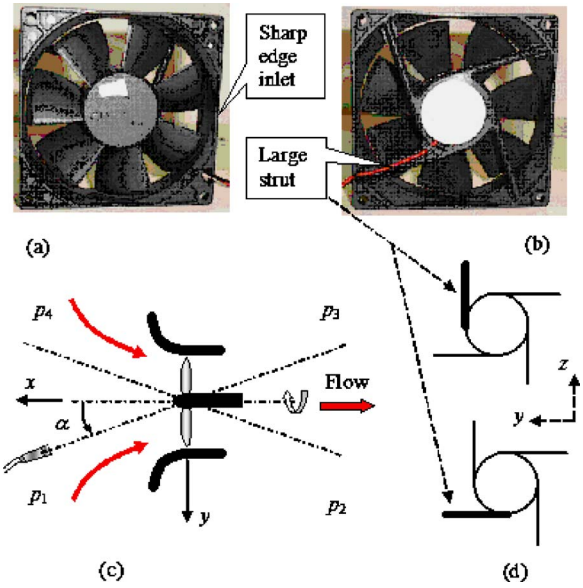

FIG. 1. (Color online) Experimental configuration. (a) and (b) The front and back views of the sample fan. (c) The top view of the horizontal measurement plane $(x-y)$ for the baseline rig. (d) The back view of two orientations of the large strut.

crophone positions, and the definition of α in the lower-left quadrant. The fan is always held in the upright position, perpendicular to the horizontal plane. It is shown in the following that the orientation of the large strut matters to the noise measured on the horizontal plane. Figure 1(b) shows the "natural" position of the large strut, while two more positions are illustrated in Fig. 1(d) in the back views of the fan (plane $y-z$). The upper drawing is for a vertical large strut and the lower one a horizontal large strut.

For such a cooling fan, Gutin noise is unlikely to be of any practical importance as the tip Mach number is of the order of 0.05. The main noise sources are the fluctuating pressures on rotor blades and struts caused by the unsteady flows. The mechanism for the broadband noise is left to future studies. For discrete tones, the following sources compete for dominance:

(1) The inlet flow distortion caused by the incomplete bellmouth frame.
(2) The tip leakage flow and the possible flow separation from both rotor blades and cylindrical struts.
(3) Scattering of unsteady boundary layer flow by the rotor trailing edges.
(4) The interaction between the rotor and downstream struts.

In terms of temporal characteristics, mechanisms 2 and 3 are not related to the fan rotation while mechanisms 1 and 4 are. If the fan rotation is accurately timed by an optical tachometer signal, the sound pressure measured by a microphone can be synchronously averaged to find the part of noise that is phase locked to the fan rotation. This part of noise is called rotary noise in the present study. The remaining sound is loosely defined as random noise although the source mechanism may have a periodical behavior. Having said that, there is a possibility of time-domain modulation by the fan rotation for mechanisms 2 and 3. For example, if the tip clearance is not uniform, fan rotation would be featured in the tip leakage flow. Due to such consideration, a baseline model is built to quantify mechanisms 2 and 3. The baseline model is illustrated in the central part of Fig. 1(c) and its construction is described as follows. First, the casing and struts of a sample fan are removed. The assembly of fan motor and rotor is mounted on a cylindrical rod extending downstream from the back of the motor. The rod has the same diameter as the motor base, and it does not cause any interference to the exit flow of the fan. A new casing with a proper bellmouth is fabricated and is held separately to form a uniform tip clearance for the rotor. Mechanisms 1 and 4 are thus excluded in the baseline model. It is shown that the baseline noise mainly features a broadband spectrum with few visible peaks. Following the same methodology, mechanisms 1 and 4 are also investigated separately by building models each being exclusive to one mechanism.

II. METHODOLOGY AND THE BASELINE CASE

In the following, the method of time-base-stretched synchronous averaging is described first, followed by the separation of the rotor-strut interaction event into drag and thrust forces by utilizing the acoustic directivity characteristics. The result of the baseline model is then analyzed together with the basic aerodynamic considerations.

A. Time-base-stretched synchronous averaging

The experiment is conducted in an anechoic chamber with a cut-off frequency of 80 Hz. The fundamental frequency of the fan noise is 350 Hz, so the laboratory environment simulates a free space. The instrumentation consists of the following components. A tachometer (B&K type M003) is used together with a stroboscope (B&K type 4913). The sample fan is installed vertically on a tripod, while a $\frac{1}{2}$ in. microphone (BSWA-MA201) is fixed at a distance of $r_0 = 0.5$ m from the fan center at a height level with the center. The tripod can be manually rotated around its vertical axis to map out the noise directivity, while the optical sensor is fixed relative to the mobile part of the tripod. The latitudinal angle α is defined in Fig. 1(c) as the angle between the rotational axis and the source-observer vector drawn from the fan center to the microphone. The microphone is calibrated by B&K's calibrator type 4231 before being used, and its signal is bandpass (200 Hz–10 kHz) filtered, and amplified by B&K's Nexus Conditioning Amplifier type 2693. The resultant signal is called the "raw" signal of sound before being further processed. The signals from the tachometer and the microphone are sampled by the National Instruments' 16-bit PCMCIA card (type SHC68-68-EP) at a rate of $F_s = 16$ kHz. Note that the required upper limit of the bandpass filter should be 8 kHz instead of 10 kHz for this choice of F_s. However, the filter design does not allow this. It is felt that this mismatch should not affect the results as trial measurement using a higher sampling rate did not show much fan noise beyond about 5 kHz. Typical traces of the two channels are shown in Fig. 2. The tachometer signal is shown in the upper part of Fig. 2(a), while the raw signal of sound is shown in the middle. The period of each rotational cycle is

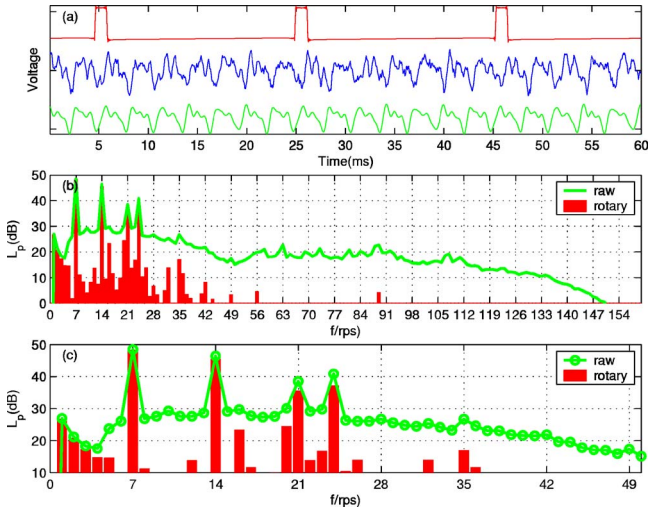

FIG. 2. (Color online) Time-base-stretched synchronous averaging. (a) The two channels of raw signals, together with the synchronously averaged wave form on the bottom part. (b) Comparison of the spectra for the raw signal with that of the averaged signal (bar chart). (c) Zoom-in view of (b).

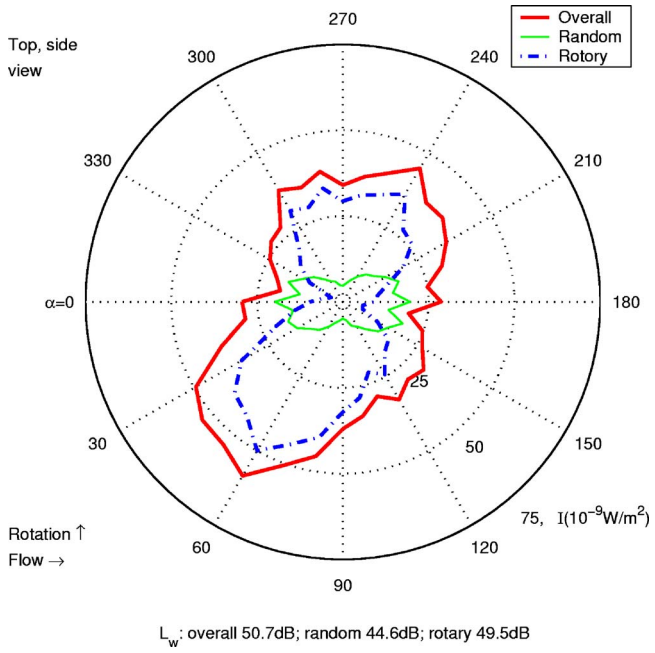

FIG. 3. (Color online) The directivity of sound intensity of all frequencies on the horizontal plane for the original fan when the large strut takes the natural position shown in Fig. 1(b).

found by the adjacent tachometer pulses. When the fan runs at a nominal speed of 3000 rpm, or 50 revolutions per second (rps), the standard deviation of instantaneous speed (rpm) is about 10–20, and the difference between two consecutive cycles is about 4 data points maximum in a total of N samples calculated as $N=\mathrm{Fs/rps}=16000/50=320$. The signals between the two rising edges of the pulses are treated as one complete rotational cycle and, during the post-data-acquisition analysis, the raw wave forms are digitally resampled to 320 points. The resampled cycles are overlapped for averaging. The result is a time-base-stretched synchronous average, and is called "rotary sound." A sample is shown in the lower part of Fig. 2(a). The duration for each data acquisition session at one measurement position is 10 s, which gives about 500 cycles for averaging. The spectrum of the raw signal is shown in Fig. 2(b) as a thick solid line, while that of the rotary sound is plotted as a bar chart. The data length for FFT is exactly one cycle, or 320, so the frequency resolution shown in the abscissa is the rotational speed (rps), and the frequency index of $B=7$ represents the BPF. Since signals below 200 Hz, or 4 rps, are contaminated by the microphone self-noise and are filtered out, the attention is focused on the noise at BPF and above. For the particular spectra shown in Fig. 2(b), the broadband noise ranges from a sound pressure level, L_p (re 20 μPa), of about 30 dB around the first BPF down to about 20 dB around the sixth BPF, while the background noise in the anechoic chamber is found to be below 10 dB based on the current spectral analysis setting. Three peaks at the frequencies of (1–3) BPF are found above the broadband level, and Fig. 2(c) provides a zoom-in view of Fig. 2(b). The difference between the raw noise power and the rotary sound power is defined as the random noise power although the underlying mechanisms might well be periodic in nature. This noise is also described as nonrotary noise in this paper. Note that the method of synchronous averaging is not new, e.g., Washburn and Lauchle (1988), but the use of the time-base stretching appears to be less common. If the results are re-processed without using the time-base stretching, random noise energy is found to be increased while the rotary noise is decreased due to the change of rotational speed for this particular fan. In other words, the energy of rotary noise "leaks" into that of random noise. For the original fan noise measured, shown later in Fig. 3, postprocessing using the time-base stretching gives an increase of 1.5 dB in rotary sound power compared with that without time-base stretching.

For a measurement point of spherical coordinates of (r_0, α, θ), where α is defined in Fig. 1(c) and θ is the rotational angle of the fan rotor, sound intensity is calculated as $I(\alpha,\theta)=p_{\mathrm{rms}}^2/\rho_0 c_0$ and the distribution of $I(\alpha)$ for a given θ is plotted as a two-dimensional directivity, $\theta=0$, π being located on the horizontal plane. The sound power is found by the integration of $I(\alpha,\theta)$ over the spherical surface of radius $r_0=0.5$ m, which is given in the following together with the definition of the sound power level, L_w,

$$W = r_0^2 \int_0^{2\pi} d\theta \int_0^{\pi} I \sin\alpha \, d\alpha,$$
$$L_w = 10 \log_{10}(W/W_{\mathrm{ref}}), \quad W_{\mathrm{ref}} = 10^{-12}\ \mathrm{W}. \tag{1}$$

Assuming that I does not change with θ, the sound power can be found by a measurement over the horizontal plane only. It is shown later that this assumption is invalid for sound generated by the interaction between the rotor and one downstream strut. In such case, more sound is generated on the horizontal plane than on other planes when the strut is placed upright, as shown in the upper drawing of Fig. 1(d). The actual sound power is between such overestimation and the underestimation produced by the horizontal plane integration when the strut is placed horizontally. Figure 3 shows the horizontal directivity of the original fan when the large strut is placed in its natural oblique position shown in Fig.

1(b). Comparisons are made later with measurements for the vertical and horizontal positions for the large strut. The solid line in Fig. 3 is the intensity of the raw noise, while the dot-dash line is the rotary sound. The difference is the so-called random noise, and is shown by a thin solid line. Note that all three sound intensity curves plotted are the result of summation over all frequencies. In this particular case, the rotary sound dominates, and the values of the sound power levels, L_w, are given in the lower horizontal label of the figure. The asymmetrical sound intensity pattern is a result of interference of sounds radiated by different unsteady force components. A brief account is given in the following for the point source formulation due to Lowson (1970) leading to the decomposition of sound pressure.

B. Point source formulation

As shown in our recent analysis (Huang, 2003), the physical size of the source can be compact, but whether the source can be described by a point source depends on the circumferential distribution of unsteady forces. Unsteady lift on airfoil, L, is decomposed into two components: thrust, T, in the direction of the rotational axis and drag, D, in the circumferential direction against the rotation. The amplitude of the far field acoustic pressure due to the rotor is found to be (Lowson, 1970)

$$C_{n=mB}^{(\mathrm{rotor})} = \frac{im\omega B^2 S}{2\pi c_0 r_0} \sum_{k=-\infty}^{\infty} i^{-\nu} e^{-i\nu\Theta} \left(T_\lambda \cos\alpha - \frac{\nu}{nM} D_\lambda \right) \times J_\nu(nM \sin\alpha), \quad \nu = n - \lambda, \quad n = mB, \quad \lambda = kS, \tag{2}$$

where T_λ and D_λ are the λth Fourier series amplitudes of the thrust and drag forces, respectively, B and S are the rotor blade and strut numbers, respectively, $M=\omega r_s/c_0$ is the rotational Mach number of the point source at radius r_s, $n=mB$ is the frequency index and m is the index of BPF harmonics, $\lambda=kS$ is the index of the source frequency, k is an arbitrary integer, and Θ is the angular position of the first strut relative to the observer on the horizontal plane of $\theta=0$. The parameter of Θ is only useful when discussing the cross-modal coupling for the single-strut noise later on. The same formula holds for sound radiated by the strut except that the source frequency λ is replaced by n since the stationary source can only radiate sound at its own frequency. Parameter ν is the index of spinning pressure mode, and it very much controls the amount of sound power radiation. The argument of the Bessel function is small, $|nM \sin\alpha| \ll 1$, so the sound radiation is only efficient when the order of the function, ν, is very low, such as $\nu=n-\lambda=0, \pm 1, \pm 2$, for which the Bessel functions can be approximated as follows:

$$J_0(z) \approx 1 - \frac{z^2}{2}, \quad J_1(z) \approx \frac{z}{2}, \quad J_{|\nu|>1} \approx \frac{1}{\sqrt{2\pi\nu}} \left(\frac{ze}{2\nu} \right)^\nu. \tag{3}$$

The thrust force does not change direction, so it radiates noise most efficiently at the frequency of the source itself, for which $\nu=0$. For the drag force, $\nu=\pm 1$ is the most efficient mode since the force component changes its direction once per cycle even when its magnitude is constant. It is shown in (Huang, 2003) that the effect of angular noncompactness is small for the leading order modes of radiation, $\nu=0, \pm 1$. For these modes, the instantaneous pressure integration for lift L suffices for the purpose of acoustic calculation.

The sound power at frequency index n is essentially the spherical integration of $|c_n|^2$ where c_n given in Eq. (2) is the sum of all possible radiation modes. Apart from the quadratic terms from each mode/force, there are two types of coupling terms. It can be shown easily that the integration of the drag-thrust coupling, a cross-component coupling, vanishes, but the coupling between different modes of the same type of force component, a cross-modal coupling, does produce sound powers. Ignoring such cross-modal coupling for the moment and assuming the independence of sound intensity on θ, the sound power is found as

$$\begin{aligned} W_n &= \int_0^\pi \frac{|c_n|^2}{2\rho_0 c_0} 2\pi r_0^2 \sin\alpha \, d\alpha \\ &= \frac{(nBS\omega)^2}{4\pi\rho_0 c_0^3} \left[\left(\frac{2}{3} T_{\lambda,\nu=0}^2 + 0.336 D_{\lambda,\nu=\pm 1}^2 \right) \right. \\ &\quad \left. + (1.07 T_{\lambda,\nu=\pm 1}^2 + 1.16 D_{\lambda,\nu=\pm 2}^2) \left(\frac{nM}{4} \right)^2 \right] \end{aligned} \tag{4}$$

in which the leading order and higher order modes are separated into two groups inside the square brackets. For the leading orders, the source radius r_s does not matter as M is absent in the sound power expression. For the less efficient, higher order modes, a factor of M^2 appears. Notice that a factor of ω^2 is also present in front of the square bracket at the right-hand side of Eq. (4). If the force magnitudes scale with the kinetic energy of flow, $T_\lambda, D_\lambda \propto M^2$, the sound power radiated is proportional to M^6 for the leading orders of ν and M^8 for the next higher orders. For $M=O(0.05)$, the higher order modes are typically 20 dB below those of the leading order modes. Assuming that there is cross-modal coupling between $\nu=0$ and $\nu=\pm 1$ for the thrust noise, the result would be a sound power which depends on M^7. The same applies to the drag noise for $\nu=\pm 1$ and $\nu=\pm 2$. However, such coupling can only occur when there is only one strut, $S=1$, as S determines the gap between the possible modal indices ν. This topic is revisited in the following when $S=1$ is investigated experimentally.

The contribution from different force components can be separated by the horizontal directivity of the radiated sound. According to Eq. (2), the leading order thrust noise is for $\nu=0$, and the sound pressure is proportional to $\cos\alpha$. This is denoted as T0 noise. The leading order drag noise has $\nu=\pm 1$ and the sound pressure features $\sin\alpha$. This is denoted as D1. The immediate higher order thrust noise is from $\nu=\pm 1$, and its directivity features $\cos\alpha \sin\alpha$. This is denoted as T1. The drag noise of $\nu=\pm 2$ has a directivity of $\sin^2\alpha$, and is denoted by D2. The patterns of the four noise components are shown in the upper row of Fig. 4, while some possible combinations of different modes are shown in the lower row

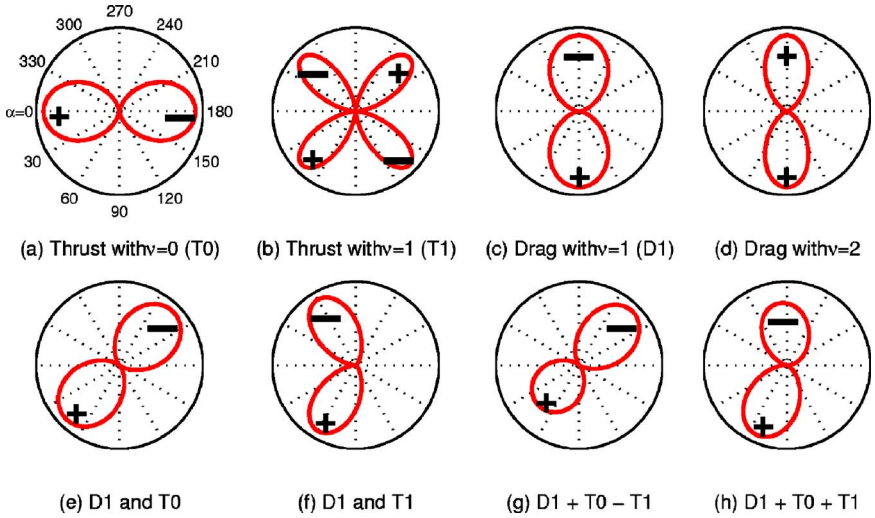

FIG. 4. (Color online) Sound intensity directivity for the most important modes (a)–(d), and a few interesting combinations. The sound pressure expressions are (a) $\cos\alpha$, (b) $\cos\alpha\sin\alpha$, (c) $\sin\alpha$, (d) $\sin^2\alpha$, (e) $\sin\alpha+\cos\alpha$, (f) $\sin\alpha+\cos\alpha\sin\alpha$, (g) $\sin\alpha+\cos\alpha-0.2\cos\alpha\sin\alpha$, (h) $\sin\alpha+0.2\cos\alpha+0.3\cos\alpha\sin\alpha$.

of Fig. 4. The labels in the main lobes denote phase angles, and the modal combinations are indicated in the coordinate labels.

Comparing phase distributions of thrust noise with drag noise, it is obvious that each has a unique feature of its own. Thrust noise changes sign across the rotational plane, while the drag noise does not. This difference, and the difference of sign between the first two quadrants of α and the other quadrants, allow the following separation of noise radiated by different force and modal components (indicated by the subscripts);

$$p_{T0}=\frac{p_1-p_2-p_3+p_4}{4},\quad p_{T1}=\frac{p_1-p_2+p_3-p_4}{4},$$
$$p_{D1}=\frac{p_1+p_2-p_3-p_4}{4},\quad p_{D2}=\frac{p_1+p_2+p_3+p_4}{4}, \tag{5}$$

where p_1,p_2,p_3,p_4 represent the synchronously averaged sound pressures measured at the four symmetrical positions in the four quadrants shown in Fig. 1(c). Note that the first quadrant is taken as the lower-left position where α ranges from 0° to 90° as shown in Fig. 1(c). This time domain separation requires a correct phase angle relation between measurements of sound at different times using the same microphone. This is achieved by fixing the tachometer relative to the fan.

The combination of different component noises can produce a huge variety of patterns, for which four are shown in the lower row of Fig. 4. Figure 4(e) shows the combination of the leading thrust noise, T0, with the leading drag noise, D0, which produces an oblique major axis of noise in the lower-left and upper-right quadrants. The directivity is nevertheless symmetrical with respect to this major axis. Figure 4(f) shows the combination of the leading mode drag noise (D1) with the higher order mode thrust noise (T1), and the result is a forward leaning directivity, which contrasts with the typical propeller noise, the latter being mainly beamed towards the rear. Figure 4(g) shows the combination of D1, D0, and T1, and the result is a pattern with a larger lobe in the upper-right quadrant than in the lower-left. Figure 4(h) shows another three-component noise with different phase angle relation, and the result is in fact the pattern found for the original fan when the large strut is in its natural position, cf. Figs. 1(b) and 3.

Shown in Fig. 5 are the experimental results for the four component noises, cf. Eq. (5), for which the overall directivity is shown in Fig. 3. In the plot of Fig. 5, the radius is the rms value of sound pressure and the scale is amplified for smaller noise components for visual clarity. The pattern shown in the lower-right quadrant is the leading mode drag noise, D1, for which the sound power level is $L_{wD1}=49.1$ dB. The lower-left quadrant shows the leading mode thrust noise, T0, which has $L_{wT0}=39.8$ dB, and the plot is magnified by five times, as indicated by the label of T0(×5). The upper-left quadrant is the higher order thrust noise with $L_{wT1}=30.2$ dB, while the upper-right quadrant is the radial noise for the mode of $\nu=0$ with $L_{wR0}=30.3$ dB. Radial noise is caused by the radial component of the unsteady forces on blades and struts, and it is excluded from

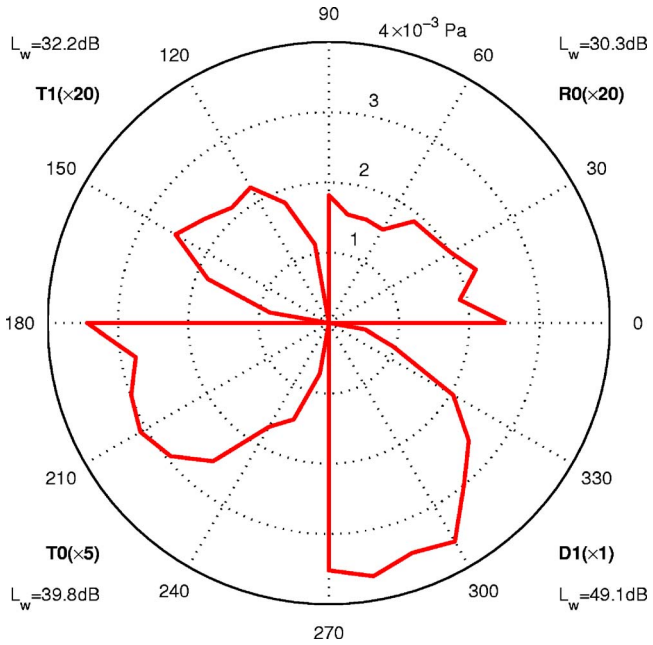

FIG. 5. (Color online) Source decomposition for the BPF noise measured for the original fan. The directivity is shown for the rms sound pressure.

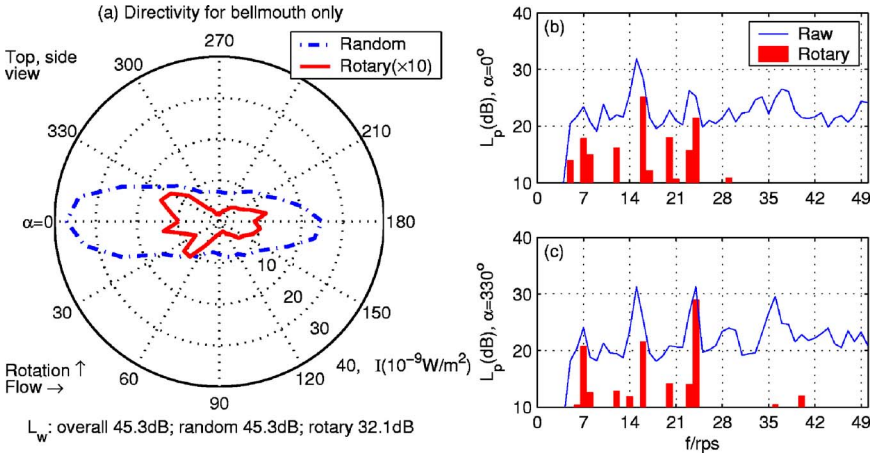

FIG. 6. (Color online) Noise from the baseline rig. (a) The directivity of random noise and rotary noise (amplified by 10 times). (b) and (c) The spectra at $\alpha=0$, 330°, respectively.

Eq. (2) as it is small for most cases considered in the current study. Radial noise could be important when the rotor or stator blades lean significantly. Details of the radial noise formulation can be found in (Huang, 2003).

C. The baseline noise

The noise made by the rotor blades alone can be investigated by a baseline case defined as the rotor blades operating in an all-clear condition with bellmouth inlet and no exit strut, the motor being supported by a solid cylinder extending downstream from the back of the motor, as illustrated in Fig. 1(c). The horizontal directivity and spectra at two latitudinal positions are shown in Fig. 6. Figure 6(a) shows that nonrotary sound (dash-dot line) dominates and the main noise axis is the rotational axis. The rotary part (solid line) is so small that it has to be amplified by ten times in terms of intensity to be seen clearly in the same plot. Noise spectra at the inlet position of $\alpha=0$ and another position of $\alpha=330°$ are shown in Figs. 6(b) and 6(c), respectively. The solid lines are for the raw noise, and the bar charts are for the synchronously averaged rotary noise. If an unsteady flow process, such as vortex shedding, is rotation-independent, it should feature in the raw noise spectrum but not much in the synchronously averaged. On the other hand, if the process is modulated by or synchronized with the rotation, the two spectra would coincide. The bar charts in Figs. 6(b) and 6(c) show that many peaks appear but most are below the broadband level of around 20 dB. Three clusters of peaks centered around 7, 16, and 24 rps are prominent. The noise at BPF =7 rps is likely to be caused by the presence of inevitable nonuniform inlet flow condition which produces regular lift fluctuations on the rotor blades. The frequencies of the peaks at 16, 24 rps, and indeed most lower peaks, are multiples of 4 rps, which may be caused by the motor vibration since there are four coils inside the brushless motor. This conjecture needs to be further validated by careful vibration measurement and analysis, which is not conducted in the present study as the peaks appearing on BPFs are dominant.

III. SINGLE- AND FOUR-STRUT RIGS

Noise radiated by the interaction between rotor blades and downstream struts can be better understood when struts are added to the baseline case in which a large inlet bellmouth is used. The following analyzes two cases, one with a single strut, denoted as S1, and another with four equal struts, denoted as S4. The case of a single strut is rather special, and its interpretation would go a long way to validating many aspects of the point source formulation presented in Sec. II. On the other hand, the case of four struts is very close to a fan of correct aeroacoustic design.

A. Single-strut interaction noise

The measured noise for S1 design is shown in Fig. 7. The strut is placed at the vertical position, as shown by the

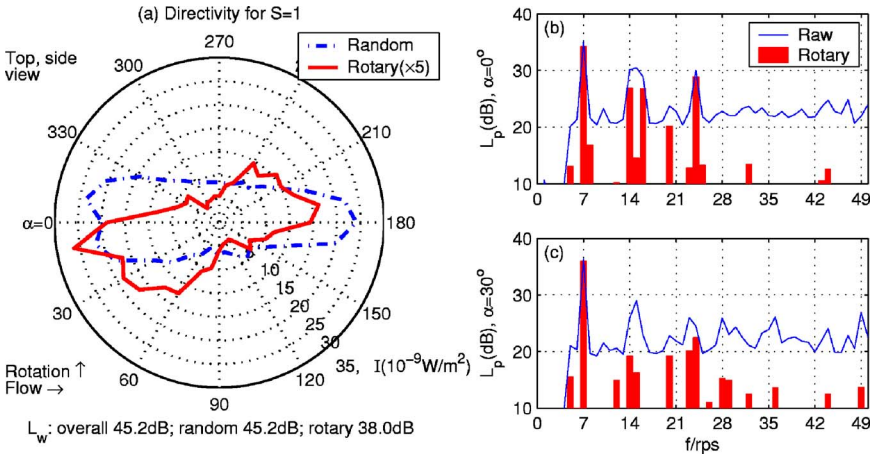

FIG. 7. (Color online) Noise radiated by a rotor interacting with a single downstream strut. (a) The directivity of rotary and non-rotary noise, (b) and (c) spectra at two important locations.

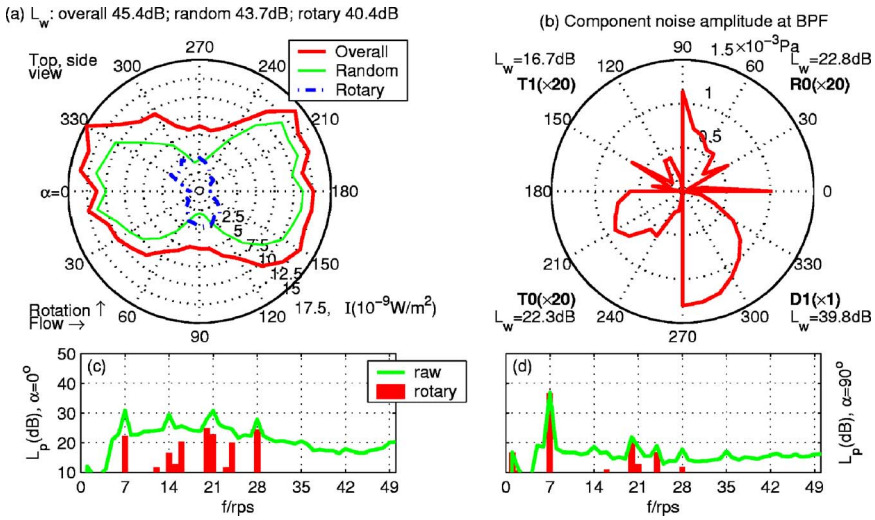

FIG. 8. (Color online) Noise radiated by a fan with four equal struts. (a) The directivity on the horizontal plane, (b) the decomposed modal directivity, (c) and (d) spectra at $\alpha=0$ and $\alpha=\pi/2$, respectively.

large strut in the upper drawing of Fig. 1(d), and the radiated noise is loudest on the horizontal plane. The rotary noise has a power of 38.0 dB, while the overall is 45.2 dB. In Fig. 7(a), the intensity for the rotary noise (solid line) is magnified by five times for visual clarity. A major rotary noise axis is found along the direction of $\alpha=30°$, and the pattern is clearly similar to Fig. 4(e) where the leading order drag noise (D1) interferes with the leading order thrust noise (T0). Figure 7(b) shows the spectrum at the inlet position of $\alpha=0$ with prominent peaks appearing at 16 and 24 rps. The highest peak is, however, at the BPF. The peak is highest for the major axis of $\alpha=30°$ in Fig. 7(c).

Recalling Eq. (2), the BPF noise radiated by the rotor with $S=1$ is found as a combination of the leading thrust mode of $\nu=0$, and the two leading modes of drag noise, $\nu=\pm1$. The combined leading order noise is

$$c_{n=B}^{(\text{rotor})}=\frac{i\omega B^2}{2\pi c_0 r_0}\left[T_7\cos\alpha+\frac{i}{2}\sin\alpha(D_6e^{-i\Theta}-D_8e^{i\Theta})\right]. \tag{6}$$

When the strut is placed on the horizontal plane, where the observer is, $\Theta=0$, and the drag noise is made by the drag magnitude of (D_6-D_8). When the strut is placed vertically, $\Theta=\pi/2$, and the source magnitude is (D_6+D_8). When considering the noise radiated by the pressure fluctuation on the strut, the source frequency has to be changed from $\lambda=kS$ to $n=B$, hence D_6 and D_8 are changed to D_7. Therefore the result for drag noise with a horizontal strut features $D_7-D_7=0$. Focusing again on the rotor noise, the major noise axis of 30° found from Fig. 7(a) means that the magnitude for thrust noise is higher than that of the drag noise. In other words, $|T_7|>|D_6+D_8|/2$. In fact, the decomposed thrust noise has $L_{wT0}=34.7$ dB, while the drag noise has $L_{w\text{D1}}=33.6$ dB.

B. Four-strut fan noise

The noise radiated by the interaction between the rotor blades and struts of equal size is investigated by using a large bellmouth at the inlet, which has been shown to be almost free from rotary noise at BPF and its harmonics. For four struts interacting with the rotor of seven blades, the theory of Eq. (2) predicts that the minimum order for the first BPF is $\nu=B-2S=-1$, implying that the drag force is the leading order noise source, while the thrust force is a higher order noise source. The measured noise radiation is shown in Fig. 8 for four struts skewed in the direction shown in Fig. 1(b) but with equal strut size. As shown by the dash-dot line of Fig. 8(a), the major rotary noise axis is along the direction of $\alpha=100°$. It is also found that most rotary noise concentrates on the BPF. The rotary noise is decomposed according to Eq. (5) and the component directivities for BPF are shown in Fig. 8(b). The leading order drag noise (D1) is shown in the lower-right quadrant and it has a power of $L_{w\text{D1}}=39.8$ dB, while the thrust noise of the first order (T1) is shown in the upper-left quadrant and it has $L_{w\text{T1}}=16.7$ dB. The comparison of these two components conforms to earlier analysis which predicts a 20 dB difference between the leading order noise and the higher order noise. However, Eq. (5) does not predict any thrust noise radiation by the mode of $\nu=0$. The actual thrust noise of this mode, shown in the lower-left quadrant of Fig. 8(b), is found to be 22.3 dB, and its combination with the drag noise determines the tilted pattern of the overall rotary intensity shown in Fig. 8(a). Such unpredicted thrust noise component could arise from the fact that not all rotor-strut interactions are wholly deterministic and identical aerodynamically, nor is the fan geometry free from any defect. Figures 8(c) and 8(d) show the spectra at the inlet and rotational plane positions. Self-noise at 16, 20, and 24 rps is also present, but the BPF noise dominates the spectrum on the rotational plane.

IV. NOISE FROM THE REAL FAN

As shown in Fig. 1, the real fan has three features which may be chiefly responsible for the noise generation: (a) the interaction between the rotor blades and the four downstream struts, which is represented above by the S4 rig, (b) incomplete bellmouth causing inlet flow distortion, and (c) the extra size of one strut which carries cables. Mechanisms (b) and (c) are now investigated separately. Mechanism (b) is represented by a configuration in which there is no strut and the motor is held by a cylindrical rod as in the baseline case,

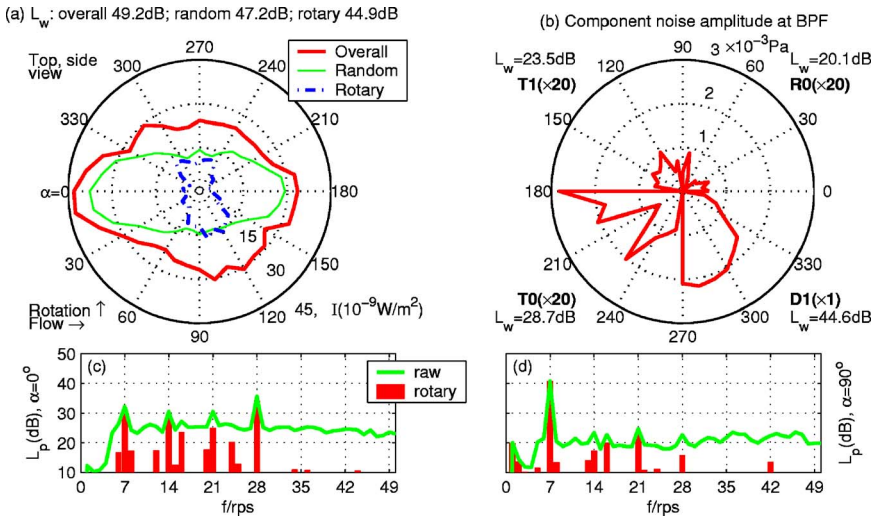

FIG. 9. (Color online) Noise radiated by the inlet flow distortion. (a) The directivity, (b) the decomposition of the radiated sound, (c) and (d) two typical spectra.

while mechanism (c) is simulated by adding an extra piece to one of the struts in the S4 rig, where a large bellmouth is installed.

A. Inlet frame noise

The presence of the four sharp edges in the incomplete inlet bellmouth is equivalent to having four upstream guide-vanes, and the formulation of Eq. (2) applies with $S=4$. The rig is denoted as IS4, and the measured noise is shown in Fig. 9, which is now compared with that from the four equal struts rig (S4) shown in Fig. 8. Figure 9(a) shows that the rotary noise of IS4 has a very similar pattern to that of S4. But the pattern of nonrotary noise is slightly different, so is the total noise. Both rotary and nonrotary noises are louder than that of S4, meaning that the inlet flow distortion is, in this case, more powerful in generating noise. This is perhaps due to the fact that the flow near the blade leading edge is more sensitive to perturbations than that near the trailing edge. The difference in the total rotary sound power is 4.5 dB while that in D1 noise power is 4.8 dB. In terms of component noise decomposition, the leading order drag noise (D1) is similar in pattern, which is shown in the lower-right quadrant of Fig. 9(b). The leading order thrust noise (T0), shown in the lower-left quadrant of Fig. 9(b), is not as regular as that in S4. Note that T0 noise derives from factors not apparent in the regular structure, and may be regarded as an indication of aerodynamic uncertainty. The difference of the T0 noise power is $28.7-22.3=6.4$ dB, which is higher than the difference in the D1 noise. This contrast also implies a more volatile aerodynamic feature for the inlet flow distortion.

B. Large strut size and orientation

Having measured the sound radiation from a single strut, cf. Fig. 7, the effect of extra strut size is investigated directly by making one of the struts in the S4 rig as large as the cable-carrying strut in the real fan sample, which is 6 mm wide in the circumferential direction and 4 mm thick in the axial direction. The large inlet bellmouth is still installed, and the large strut is held upright, as shown in the upper drawing of Fig. 1(d), while the directivity is measured on the horizontal plane. The rig is denoted as S13, implying one large strut with 3 regular struts. The measured noise is shown in Fig. 10. The nonrotary noise is shown as a thin solid line in Fig. 10(a). The power is 45.2 dB, and it has a tilted pattern very similar to the rotary noise shown as the dash-dot line. For the rotary noise, the difference between the S13 rig and the S4 rig represents the extra noise caused by the extra strut size. The extra noise consists of the extra drag noise, which is shown in the S1 study to be proportional to $|D_6+D_8|$, and the extra thrust noise proportional to T_7. As shown in the title of Fig. 10(b) for the BPF, the T0 noise is 39.7 dB, which is much higher than the 22.3 dB found in the S4 rig, the latter being unaccounted for from structural view point. Since the S4 noise is drag-dominated, this 39.7 dB should all be attributed to the so-called extra noise, and it is almost the same as the 39.8 dB drag noise found in the S4 rig. The leading mode drag noise, D1, for the present rig has 44.3 dB, which is much higher than the 39.8 dB from the S4 rig, but slightly lower than the 44.6 dB from the IS4 rig. A level-ground interference is expected for the D1 noise in the S4 rig and the extra drag noise.

The extra noise from the large strut is also responsible for the tilting of the major noise axis from around the rotational plane to about $\alpha=50°$. But the more striking feature of the rotary noise, shown as the dot-dash line in Fig. 10(a), is the difference between the lobes in the lower-left and upper-right quadrants, which is similar to that shown in Fig. 4(g). The best fit for the rotary BPF component is found by the following sound pressure expression:

$$p = \underbrace{4.628 \sin\alpha}_{D1} + \underbrace{3.858 \cos\alpha}_{T0} - \underbrace{0.965 \cos\alpha \sin\alpha}_{T1} (\times 10^{-3}\ \text{Pa}). \quad (7)$$

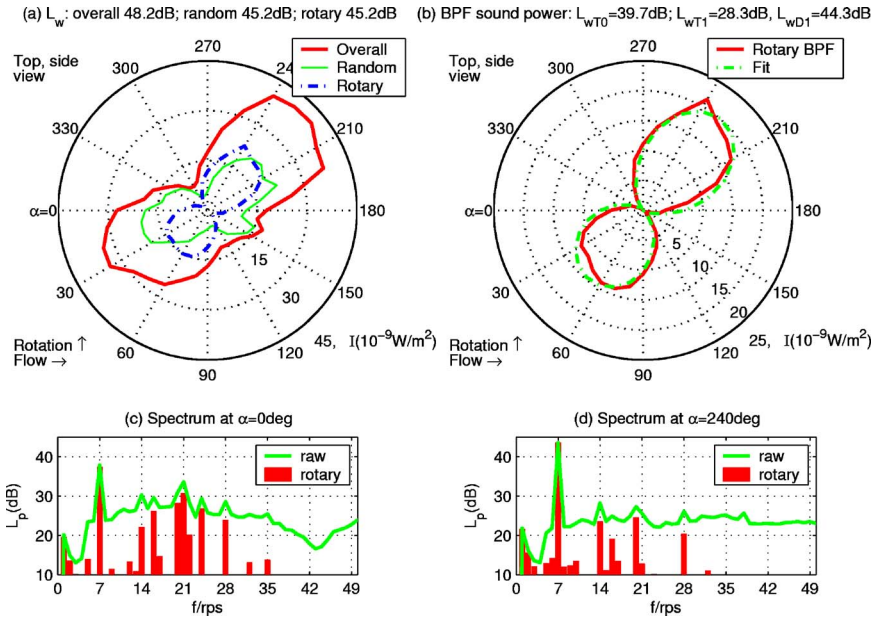

FIG. 10. (Color online) Noise radiated by the interaction of rotor blades with four struts in which one is larger than the others. (a) The overall directivity when the large strut is in the natural oblique position, (b) the effect of large strut orientation, (c) and (d) two typical spectra for (a).

The D1 noise is apparently derived from the drag noise from the interaction between the rotor and the four struts, the T0 noise is from the effect of the large strut, i.e., the extra noise, and the higher order thrust noise (T1) is derived from either the S4 noise or the extra noise. The sound power for T1 is 28.3 dB, which is much higher than the corresponding 16.7 dB from the S4 rig shown in Fig. 8(b). Again, the effect of the extra strut size is found to be dominant. The spectra on the major noise axis of α=0°, 240° are shown in Figs. 10(c) and 10(d), respectively, and both show a clear dominance of the BPF component.

The effect of the large strut orientation is investigated for the original fan by turning the direction of the large strut from the vertical to horizontal direction, cf. Fig. 1(d), while the directivity is measured on the fixed horizontal plane. The comparison of the rotary noise directivities is shown in Fig. 11. Recalling from Eq. (1) that the sound power integration should be carried out over the whole spherical surface, i.e., over both α and θ, it is pointed out that the current α-integration on the horizontal plane represents an approximation based on the assumption that the noise distribution on planes parallel to the rotational planes is uniform. The approximate sound power level obtained from the measurement when the large strut is in the vertical position, shown as the dash-dot line of Fig. 10(b), is certainly higher than that in the horizontal position, shown as the solid line, and the difference of rotary noise is 2.9 dB. In order to make a proper evaluation of the true sound power, measurement should be made over the whole sphere in this case instead of over the central horizontal plane. The approximate result obtained for the data taken at the oblique, or natural, position of the large strut, shown in Fig. 1(b), is probably closer to the true value than those from the two extreme orientations of the large strut shown in Fig. 1(d). The rotary noise for such natural position of the large strut is 49.5 dB. Comparing this rotary noise of 49.5 dB with the 40.1 dB from the rig with four equal struts (S4), one can see a potential of 9.4 dB noise reduction. The rotary sound powers made by the inlet flow distortion (IS4) and the unequal set of four struts (S13) are both around 45 dB. In order to eradicate both, the inlet bellmouth and the large strut size have to be corrected. Extra structural considerations are needed to achieve this. Although such corrections may mean extra manufacturing cost, the large noise reduction may well compensate for this.

V. CONCLUSIONS

Experimental analysis of a typical computer cooling fan noise has revealed many interesting features, and the understanding derived is expected to be helpful in devising quiet fans. For the sample fan used in the current study, a 9.4 dB noise abatement potential is identified. However, the focus of this study is on the directivity analysis of the radiated sound. The following conclusions are made.

(1) Time-base stretched synchronous averaging has been used to extract the part of noise which is phase locked to

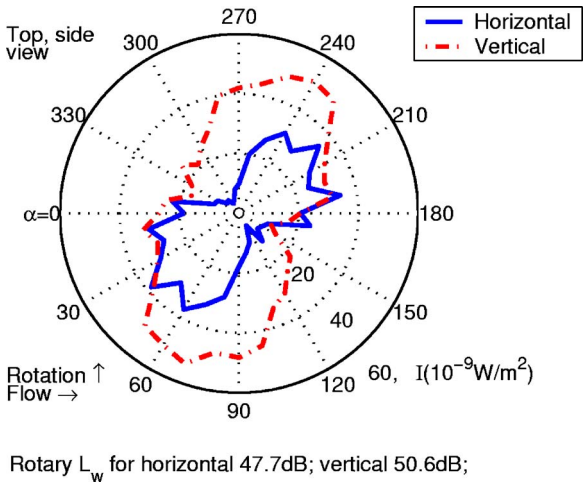

FIG. 11. (Color online) Effect of the large strut orientation for the original fan.

the fan rotation. The nonrotary part of the noise is found to be broadband in nature. However, within the rotary noise, there are peaks which do not coincide with the blade passing frequency and its harmonics. These peaks form a series of harmonics of 4 rps, which is probably caused by the vibration of the motor which has four coils. The contribution from such peaks to the total noise is small except in directions where the rotary sound is weak.

(2) The rotary noise radiated by the interaction between the rotor blades and the downstream struts or the upstream flow distortions can be understood within the framework of point source formulation of Lowson (1970). The effect of noncompactness is considered to be small. This is not purely because of the small size of the fan, but due to the fact that the leading radiation modes have an index of spinning pressure modes close to $\nu=0$. Noise from $|\nu|>1$ can be neglected, such as the Gutin noise.

(3) Based on the phase angle characteristics, the measured sound can be decomposed into four parts as a combination of two unsteady forces, drag and thrust, and two modes, $\nu=0$ and $|\nu|=1$. Results from such decomposition analysis have been interpreted within the framework of point source formulation.

(4) For the sample fan of seven rotor blades and four struts, the drag noise of $\nu=-1$ dominates. Structural decomposition shows that the noise radiated by the inlet flow distortion is equivalent to having four upstream guidevane and the noise radiated is found to be even higher than that from the interaction between the rotor blades and the four equal struts when a proper inlet bellmouth is installed.

(5) The large strut is found to cause a lot of extra noise. The extra noise has features similar to the noise radiated by the rotor interacting with one single strut, a configuration which is also studied. The extra noise is divided into extra thrust noise derived from the Bth Fourier component of the thrust fluctuation, T_B, and extra drag noise, which features a combination of two spectral components in different combinations, $D_{B-1}\pm D_{B+1}$, depending on the orientation of the strut. For the sample fan, the extra drag noise couples with the four-strut drag noise, and the result is a 5 dB increase. Trimming of the large strut size can reduce noise by 5 dB, so does the smoothing out of the inlet bellmouth.

(6) Combinations of component noise give a variety of total rotary noise patterns. All measured directivity can be interpreted as a sum of leading order drag and thrust noises, plus a higher order thrust noise which plays a subtle role in altering the outlook of the acoustic directivity.

ACKNOWLEDGMENTS

The project is funded by a Competitive Earmarked Research Grant from the Hong Kong SAR Government (Account B-Q439, RGC S/N: PolyU 5162/01E). J.W. also wishes to acknowledge the support of the PhD research studentship from the Hong Kong Polytechnic University.

Blake, W. K. (**1986**). *Mechanics of Flow-induced Sound and Vibration* (Academic, New York).

Curle, N. (**1955**). "The influences of solid boundaries upon aerodynamic sound," Proc. R. Soc. London, Ser. A **A231**, 505–514.

Ffowcs Williams, J. E., and Hall, L. H. (**1970**). "Aerodynamic sound generation by turbulent flow in the vicinity of a scattering half-plane," J. Fluid Mech. **40**, 657–670.

Ffowcs Williams, J. E., and Hawkings, D. L. (**1969**). "Sound generation by turbulence and by surfaces in arbitrary motion," Philos. Trans. R. Soc. London, Ser. A **A264**, 321–342.

Fitzgerald, J. M., and Lauchle, G. C. (**1984**). "Reduction of discrete frequency noise in small, subsonic axial-flow fans," J. Acoust. Soc. Am. **76**, 158–166.

Fukano, T., Takamatsu, Y., and Kodama, Y. (**1986**). "The effects of tip clearance on the noise of low pressure axial and mixed flow fans," J. Sound Vib. **105**, 291–308.

Gutin, L. (**1936**). "On the sound field of a rotating propeller," NACA TM 1195 (translated in 1948 from *Zhurnal tekhnicheskoĭ fiziki* **6**, 899–909).

Howe, M. S. (**1998**). "Trailing edge noise at low Mach numbers," J. Sound Vib. **225**, 211–238.

Huang, L. (**2003**). "Characterizing computer cooling fan noise," J. Acoust. Soc. Am. **114**, 3189–3200.

Kaji, S., and Okazaki, T. (**1970**). "Generation of sound by rotor-stator interaction," J. Sound Vib. **13**, 281–307.

Kemp, N. H., and Sears, W. R. (**1953**). "Aerodynamic interference between moving blade rows," J. Aeronaut. Sci. **20**, 583–598.

Kemp, N. H., and Sears, W. R. (**1955**). "Unsteady forces due to viscous wakes in turbomachines," J. Aeronaut. Sci. **22**, 478–483.

Lighthill, M. J. (**1952**). "On sound generated aerodynamically: I. General theory," Proc. R. Soc. London, Ser. A **A211**, 564–587.

Longhouse, R. E. (**1976**). "Noise mechanism separation and design considerations for low tip-speed, axial-flow fans," J. Sound Vib. **48**, 461–474.

Longhouse, R. E. (**1977**). "Vortex shedding noise of low tip speed, axial flow fans," J. Sound Vib. **53**, 25–46.

Longhouse, R. E. (**1978**). "Control of tip-vortex noise of axial flow fans by rotating shrouds," J. Sound Vib. **58**, 201–214.

Lowson, M. V. (**1970**). "Theoretical analysis of compressor noise," J. Acoust. Soc. Am. **47**, 371–385.

Majumdar, S. J., and Peake, N. (**1998**). "Noise generation by the interaction between ingested turbulence and a rotating fan," J. Fluid Mech. **359**, 181–216.

Morfey, C. L. (**1973**). "Rotating blades and aerodynamic sound," J. Sound Vib. **28**, 587–617.

Mugridge, B. D., and Morfey, C. L. (**1972**). "Sources of noise in axial flow fans," J. Acoust. Soc. Am. **51**, 1411–1426.

Quinlan, Q. A., and Bent, P. H. (**1998**). "High frequency noise generation in small axial flow fans," J. Sound Vib. **218**, 177–204.

Sharland, I. J. (**1964**). "Sources of noise in axial flow fans," J. Sound Vib. **1**, 302–322.

Trunzo, R., Lakshminarayana, B., and Thompson, D. E. (**1981**). "Nature of inlet turbulence and strut flow disturbances and their effect on turbomachinery rotor noise," J. Sound Vib. **76**, 233–259.

Tyler, J. M., and Sofrin, T. G. (**1962**). "Axial flow compressor noise studies," Soc. Autom. Eng. Trans. **70**, 309-332.

Washburn, K. B., and Lauchle, G. C. (**1988**). "Inlet flow conditions and tonal sound radiation from a subsonic fan," Noise Control Eng. J. **31**, 101–110.